

# TransUNet-GradCAM: A Hybrid Transformer-U-Net with Self-Attention and Explainable Visualizations for Foot Ulcer Segmentation

Akwasi Asare <sup>1\*</sup>, Mary Sagoe <sup>1</sup>, Justice Williams Asare<sup>1</sup>, Stephen E. Moore<sup>2</sup>

<sup>1</sup>*Department of Computer Science, Faculty of Computing and Information Systems, Ghana Communication Technology University, Accra, Ghana*

<sup>2</sup>*Department of Mathematics, University of Cape Coast, Cape Coast, Ghana*

**Corresponding Author:** [nasare34@yahoo.com](mailto:nasare34@yahoo.com)

**Abstract:** Automated segmentation of diabetic foot ulcers (DFUs) plays a critical role in clinical diagnosis, therapeutic planning, and longitudinal wound monitoring. However, this task remains challenging due to the heterogeneous appearance, irregular morphology, and complex backgrounds associated with ulcer regions in clinical photographs. Traditional convolutional neural networks (CNNs), such as U-Net, provide strong localization capabilities but struggle to model long-range spatial dependencies due to their inherently limited receptive fields. To address this, we employ the TransUNet architecture, a hybrid framework that integrates the global attention mechanism of Vision Transformers (ViTs) into the U-Net structure. This combination allows the model to extract global contextual features while maintaining fine-grained spatial resolution. We trained the model on the public Foot Ulcer Segmentation Challenge (FUSeG) dataset using a robust augmentation pipeline and a hybrid loss function to mitigate class imbalance. On the internal validation set, the model achieved a Dice Similarity Coefficient (F1-score) of 0.8886 using an optimized threshold of 0.4843. Crucially, to assess generalizability, we performed external validation on two independent datasets: the AZH Wound Care Center dataset (n=278) and the Medetec dataset (n=152). Without any retraining, the model achieved Dice scores of 0.6209 and 0.7850, respectively, demonstrating robust zero-shot transferability to unseen clinical domains. Furthermore, clinical utility analysis revealed a strong correlation (Pearson  $r = 0.9749$ ) between predicted and ground-truth wound areas. These outcomes demonstrate that our approach effectively integrates global and local feature extraction, offering a reliable, effective, and explainable solution for automated foot ulcer assessment.

**Keywords:** Diabetic Foot Ulcer Segmentation, TransUNet, Vision Transformer (ViT), U-Net, Wound Assessment, Explainable Deep Learning (Grad-CAM)

## 1. Introduction

Non-healing wounds, both acute and chronic, impose a significant burden on global healthcare systems, impacting millions of individuals each year [1]. In the United States, estimated Medicare costs associated with all types of wounds range widely, from \$28.1 billion to \$96.8 billion [2]. A key distinction lies with chronic wounds, which unlike acute wounds, do not progress through the healing stages in a predictable or timely manner [1]. This often necessitates hospitalizations and additional medical interventions, adding billions to annual healthcare expenditures [1,3]. Furthermore, a shortage of adequately trained wound care specialists, particularly in primary and rural settings, restricts access to quality care for a large segment of people [1,4]. For the effective evaluation and management of chronic wounds, precise measurement of the wound area is fundamental [1,5,6]. This measurement is crucial for tracking healing progress and guiding future treatment decisions [6]. However, current manual measurement techniques are laborious and frequently inaccurate, which can negatively affect patient outcomes [7]. Automated wound segmentation from medical images offers a compelling solution, not only by automating the measurement of wound area but also by enabling efficient data integration into electronic medical records, thereby improving overall patient care [8,9].

Diabetes mellitus (DM) is a long-term illness that demands continuous management, extending beyond just monitoring blood glucose levels and it currently affects millions worldwide, with projections indicating that the global number of cases may surpass 700 million by 2050 [9]. Diabetic foot ulcers (DFUs) represent a severe complication of diabetes mellitus, affecting millions worldwide and often leading to significant morbidity, lower limb amputations, and increased mortality rates [10,11]. Their early and precise assessment is paramount for effective clinical management, encompassing accurate diagnosis, personalized treatment strategies, and continuous wound monitoring [10]. Manual segmentation of these ulcers from clinical images, however, is a time-consuming and subjective process, heavily reliant on expert experience [12,13]. This manual approach is also prone to inter-observer variability and errors, which can hinder consistent and objective evaluation of wound healing progression [13]. However, the automated segmentation of DFUs from clinical images remains a complex task due to the considerable variability in their appearance, shape, and contextual presentation. Deep learning, a subset of Artificial intelligence (AI) has indeed revolutionized medical imaging analysis and is rapidly transforming healthcare [14–16]. While deep learning, particularly convolutional neural networks (CNNs) like the U-Net architecture, has transformed medical image analysis and provided automated solutions for various segmentation challenges, these models primarily rely on local convolutional operations [17,18]. This inherent characteristic often restricts their effectiveness in capturing long-range spatial dependencies and global contextual information across an entire image [19]. For DFU segmentation, where ulcer characteristics can differ widely, comprehending the broader context of the wound and surrounding tissues is vital for accurate delineation.

To address the limitations of purely convolutional architectures in capturing global dependencies, recent advancements have introduced Vision Transformers (ViTs) to the field of image analysis. Transformers, originally developed for natural language processing, excel at modeling extensive relationships through their self-attention mechanisms [20]. Concurrently, emerging paradigms such as in-context learning have demonstrated potential for few-shot medical segmentation by leveraging visual prompts to adapt to new tasks with minimal data [21,22]. While these approaches offer flexibility, high-stakes clinical tasks like DFU assessment demand the stability, consistency, and specialized feature extraction that supervised training on large, domain-specific datasets

provides. Integrating these capabilities for global feature extraction with the precise localization power of U-Net presents a compelling approach for enhancing medical image segmentation.

In this paper, we employ the TransUNet architecture, a hybrid framework that merges the global contextual understanding of Vision Transformers with the precise localization power of U-Net. We specifically enhance this framework with a robust data augmentation pipeline designed to handle the significant illumination and skin-tone variability found in clinical DFU photography. Furthermore, we integrate Grad-CAM visualizations to provide explainable insights into the model's decision-making process. We evaluate our approach on the Foot Ulcer Segmentation Challenge (FUSeg) dataset, demonstrating that the synergistic combination of Transformer-based global attention and CNN-based local detail preservation yields reliable and effective segmentation performance. The rest of this paper is organized as follows: Section 2 presents the materials and methods used, detailing the TransUNet architecture, the FUSeg dataset, and the evaluation metrics. Section 3 presents the quantitative and qualitative results. Section 4 provides a discussion of the findings, and Section 5 concludes the paper by summarizing our contributions and outlining future research directions.

## **2. Materials and Methods**

### **2.1 Dataset**

In this study, we utilized the Foot Ulcer Segmentation Challenge (FUSeg) dataset, a publicly available benchmark curated under the MICCAI framework [1,23]. This dataset focuses on the semantic segmentation of foot ulcer regions in clinical photographs, aiming to support automated wound assessment in real-world healthcare scenarios. The dataset comprises over 1,200 high-resolution images, captured over a two-year period from hundreds of patients during routine medical evaluations as seen in Figure 3. All images are de-identified in accordance with HIPAA guidelines to protect patient privacy.

The dataset is systematically divided into three subsets: training, validation, and testing.

- a) **Training Set:** Includes 810 images with corresponding expert-annotated segmentation masks (see Figure 1), used for model optimization.
- b) **Validation Set:** Contains 200 image-mask pairs. This set was used for hyperparameter tuning, model checkpointing, and the quantitative performance evaluation (Dice, IoU) reported in Table 1.
- c) **Test Set:** Comprises 200 unlabeled images reserved exclusively for blind evaluation and leaderboard submission. Since ground truth masks are not provided for this split, it was utilized solely for qualitative visual assessment and generating submission predictions.

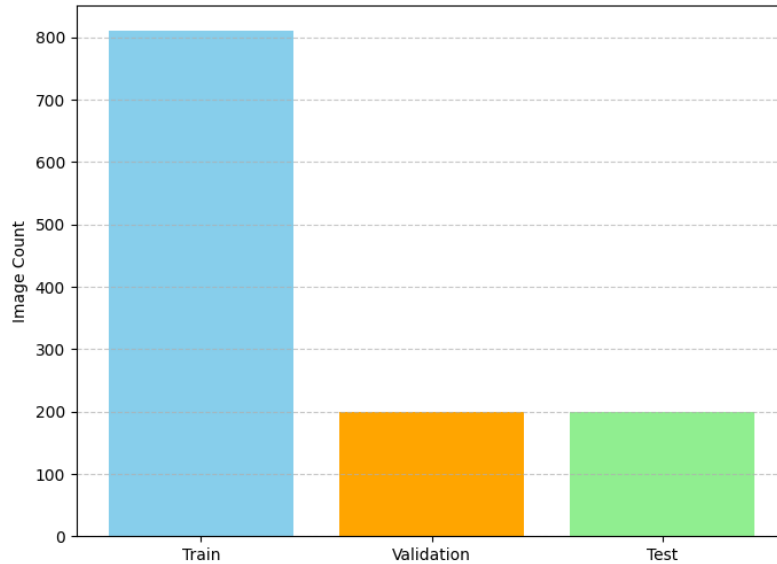


Figure 1. Number of images per Dataset split

All data are organized in structured directories, with separate folders for input images and ground truth masks. For model inference, the trained TransUnet model generated probabilistic predictions that were binarized using a threshold of 0.5. Pixels predicted as ulcer regions were assigned a grayscale value of 255, while background pixels were assigned 0. These binary segmentation masks were saved with consistent naming for traceability and evaluation purposes.

Figure 2 shows the pixel intensity distribution of sample images and the corresponding segmentation mask class frequencies, highlighting the predominance of background pixels (value 0) and the relatively smaller proportion of wound regions (value 255).

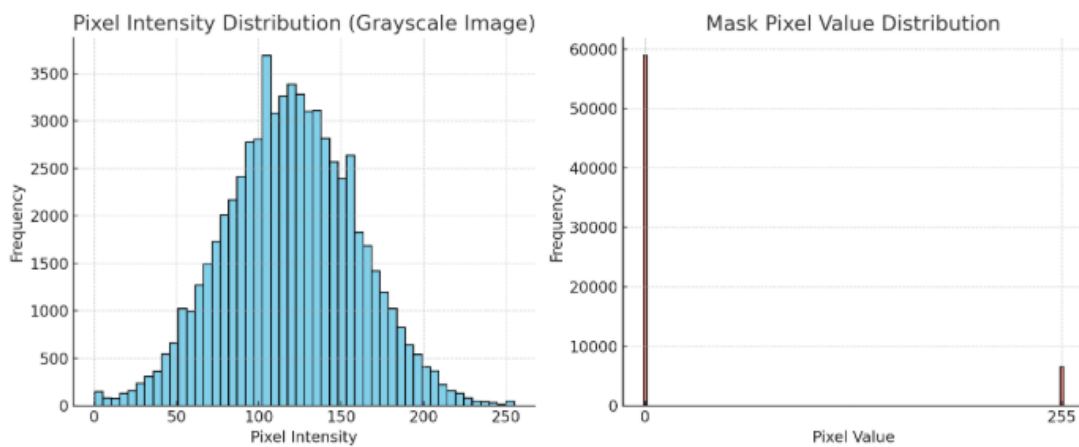
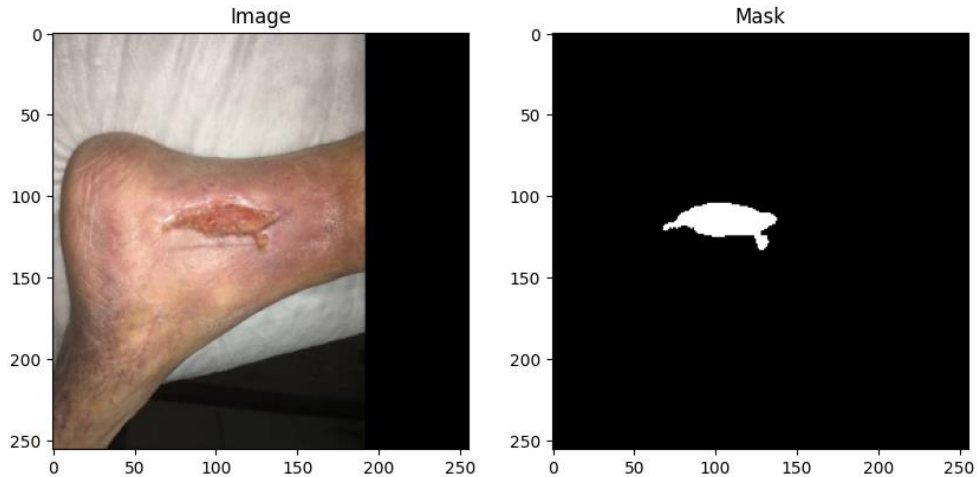


Figure 2: Pixel Intensity Distribution and Mask Pixel Value Distribution



*Figure 3: Sample dataset visualization- Image and its corresponding mask*

External Validation Datasets: To evaluate the model’s robustness against domain shifts (e.g., differences in camera sensors, lighting, and wound presentation), we utilized two independent external datasets:

- a) AZH Wound Care Center Dataset: A distinct cohort comprising 278 wound patch images acquired from a different clinical setting [24].
  - b) Medetec Dataset: An additional external dataset consisting of 152 wound images [25,26].
- These datasets served strictly as external testing cohorts; the model was never trained or fine-tuned on these images, ensuring a thorough assessment of its generalization capabilities.

## **2.2 Model Architecture and Training Details**

In this work, we employed the TransUNet architecture, a hybrid semantic segmentation framework that effectively merges the strengths of convolutional neural networks (CNNs) and Vision Transformers (ViTs). This design addresses the inherent limitations of pure CNNs in capturing long-range dependencies. The architecture is specifically selected for medical image segmentation, offering a synergistic blend of local feature representation through CNN encoders and global context modeling via transformer-based attention mechanisms. All clinical RGB images, initially acquired at a resolution of  $512 \times 512 \times 3$ , were rescaled to  $256 \times 256 \times 3$  pixels to minimize computational complexity and GPU memory usage while maintaining sufficient anatomical detail.

### **2.2.1 Convolutional Encoding Blocks**

The encoder component is constructed using sequential convolutional blocks, each comprising two 2D convolutional layers with a kernel size of  $3 \times 3$  and ‘same’ zero padding. These layers are followed by batch normalization and ReLU activation. The convolutional blocks hierarchically extract low- to mid-level spatial features. Each encoding block is followed by a  $2 \times 3$  max pooling operation to downsample feature maps and expand the receptive field.

## 2.2.2 Transformer Bottleneck Module

To overcome the local receptive field limitation of CNNs, a Vision Transformer module is integrated at the bottleneck. The deepest convolutional feature map (p4) is reshaped into a sequence of non-overlapping 2D patches, each of size 1 x 1 pixel (effectively treating each feature map pixel as a token). These patches are flattened and projected into a fixed-dimensional embedding space. To retain positional context, learnable positional encodings are added to the token embeddings. The transformer block consists of six sequential Transformer encoder layers, each composed of a Multi-Head Self-Attention (MHSA) mechanism with 8 heads and a Feed-Forward Network (FFN). This mechanism enables the model to capture global relationships between distant image regions.

## 2.2.3 Decoder and Skip Connections

The decoder reconstructs the full-resolution segmentation mask by progressively up-sampling the feature maps. Each decoder stage concatenates the up-sampled features with the corresponding encoder feature map via skip connections. These connections act as direct pathways for spatial information, facilitating fine-grained localization of wound boundaries. At the final layer, a 1 x 1 convolution with a sigmoid activation function is employed to project the output to a single probability channel.

## 2.2.4 Complete Network Construction

The full architecture follows an encoder–transformer–decoder pipeline as illustrated in Figure 4. The encoder comprises four stages, doubling the number of filters from 32 to 256. The bottleneck processes the deepest features via the Transformer module. The decoder mirrors the encoder with four up-sampling stages, restoring the resolution to 256 x 256. A Grad-CAM module is used for visualization, with gradient signals backpropagating from the segmentation output to the feature maps.

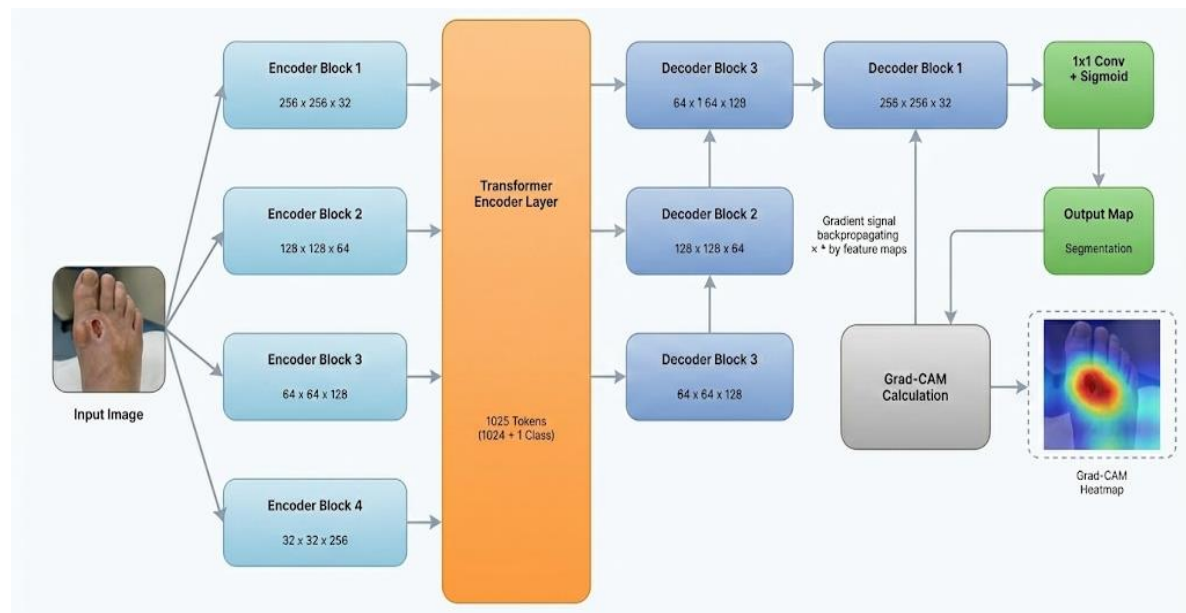


Figure 4: The proposed TransUNet hybrid architecture for diabetic foot ulcer segmentation

## 2.3 Evaluation Metrics

To quantitatively assess segmentation performance on the validation set, we employed standard metrics:

1. **Dice Similarity Coefficient (DSC)**: Measures the harmonic mean of precision and recall (F1-score), quantifying the overlap between the predicted segmentation  $Y_{pred}$  and the ground truth mask  $Y_{true}$  [27]. It is defined as:

$$DSC = \frac{2 \cdot |Y_{pred} \cap Y_{true}|}{|Y_{pred}| + |Y_{true}| + \epsilon} \quad (1)$$

A Dice score close to 1.0 signifies high segmentation accuracy and is particularly useful when the target class occupies a small portion of the image.

2. **Intersection over Union (IoU)**: Also referred to as the Jaccard Index, IoU calculates the ratio of the intersection to the union of the predicted and ground truth masks [28].

$$IoU = \frac{|Y_{pred} \cap Y_{true}|}{|Y_{pred} \cup Y_{true}| + \epsilon} \quad (2)$$

1. **Pixel Accuracy**: The proportion of correctly classified pixels over the entire image. [29–31].

$$Accuracy = \frac{TP + TN}{TP + TN + FP + FN} \quad (3)$$

where TP, TN, FP, and FN represent true positives, true negatives, false positives, and false negatives, respectively. The small constant  $\epsilon = 10^{-6}$  ensures numerical stability during division.

## 2.4 Training Strategy and Advanced Augmentation

Model compilation was performed using the Adam optimization algorithm with an initial learning rate of  $1 \times 10^{-4}$ . To address the inherent variability in clinical DFU images, particularly regarding illumination and skin tone, we implemented a robust data augmentation pipeline using the `imgaug` library. During training, images underwent on-the-fly geometric transformations (random rotations  $\pm 45^\circ$  horizontal/vertical flips) and photometric perturbations (random brightness/contrast adjustments, Gaussian blur). Critically, we applied Color Jitter (Hue/Saturation shifts) to simulate diverse skin pigmentation and lighting conditions.

To mitigate class imbalance between the small ulcer regions and the extensive background, we employed a Hybrid Loss function combining Binary Cross-Entropy (BCE) and Dice Loss:

$$L_{total} = L_{BCE} + (1 - Dice) \quad (4)$$

Training was conducted for a maximum of 100 epochs with a batch size of 16. We utilized `ModelCheckpoint` to save the best weights based on validation loss [32], `ReduceLROnPlateau` [33]

to decay the learning rate by a factor of 0.5 upon stagnation, and *EarlyStopping* [34] with a patience of 12 epochs to prevent overfitting. All validation steps were deterministic (no augmentation) to ensure consistent metric reporting.

### 3. Results

This section presents the quantitative and qualitative evaluation of the TransUNet-GradCAM framework. The model's performance was assessed using standard metrics-Dice Similarity Coefficient (DSC), Intersection over Union (IoU), and Accuracy calculated on the local validation set for which ground truth masks were available.

#### 3.1 Training Dynamics and Stability

The training process was conducted for a maximum of 100 epochs to ensure full convergence of the hybrid architecture. As illustrated in Figure 5, the model demonstrated highly stable learning behavior. The validation loss progressively decreased from an initial high of 58.38 to a minimum of 0.1315. The optimal model weights were restored from Epoch 99, which corresponded to the best generalization performance. The consistent alignment between training and validation curves indicates that the robust augmentation pipeline effectively prevented overfitting.

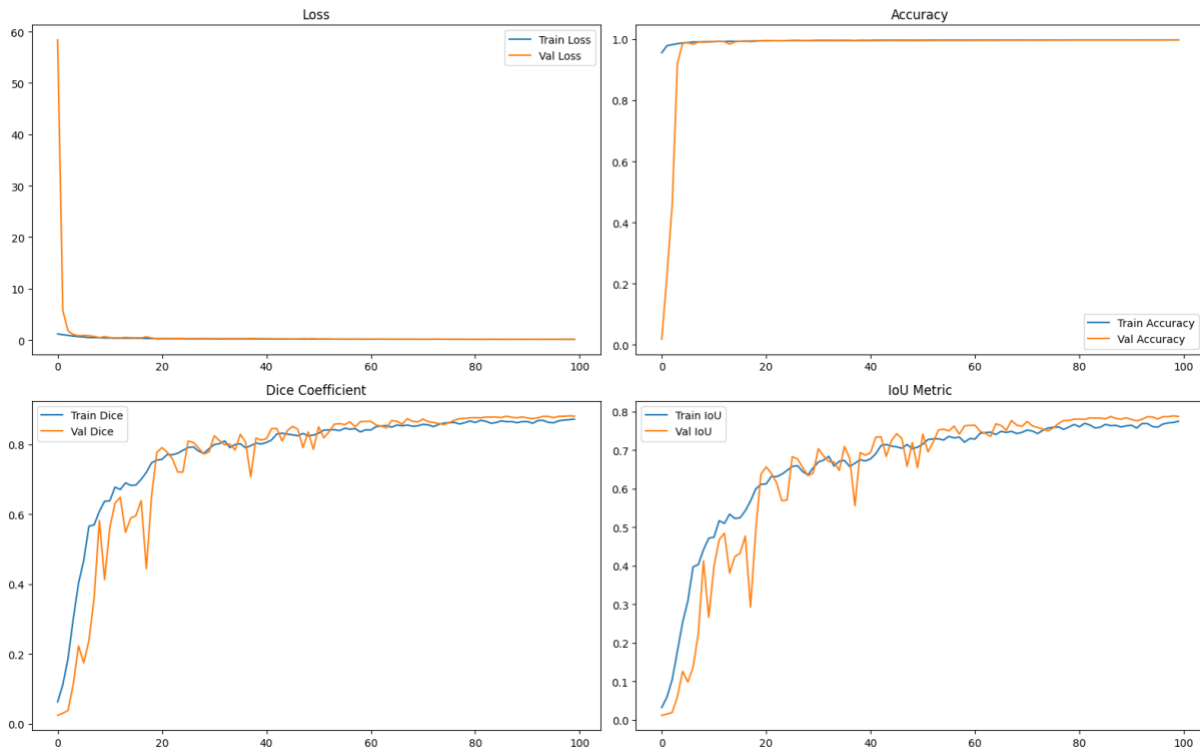


Figure 5: Training and validation metrics over 100 epochs. The curves demonstrate stable convergence, with the optimal checkpoint identified at Epoch 99.

#### 3.2 Quantitative Performance

Table 1 summarizes the performance metrics on the validation set based on the optimal checkpoint (Epoch 99). The proposed framework achieved a validation Dice Coefficient (F1-score) of 0.8886 and an IoU of 0.7889. These results represent a significant improvement over standard baselines, validating the efficacy of the hybrid CNN-Transformer design.

Table 1: Performance Metrics on the Training Set (n=810) and the Local Validation Set (n=200).

| Metric          | Training Value | Validation Value |
|-----------------|----------------|------------------|
| Accuracy        | 0.9969         | 0.9973           |
| IoU (Jaccard)   | 0.7757         | 0.7889           |
| Dice (F1 Score) | 0.8726         | 0.8886           |
| Loss            | 0.1422         | 0.1315           |

### 3.3 Advanced Quantitative Evaluation

To rigorously assess the model's discriminative capability beyond standard metrics, we performed a threshold optimization analysis on the validation set. While the default decision boundary of 0.5 yielded strong performance, a comprehensive sweep across potential thresholds (0.0 to 1.0) identified an optimal threshold of 0.4389. Applying this optimized threshold maximized the F1-score (Dice Coefficient) to 0.8799, demonstrating that fine-tuning the binarization strategy can yield measurable improvements in segmentation accuracy. This suggests the model is well-calibrated, as the optimal threshold is very close to the standard 0.5 decision boundary.

The model's robustness is further substantiated by the Receiver Operating Characteristic (ROC) and Precision-Recall (PR) curves presented in Figure 6. The high Area Under the Curve (AUC) indicates that the model maintains high sensitivity and specificity even when processing complex wound images with challenging backgrounds, effectively distinguishing ulcerated tissue from healthy skin and artifacts.

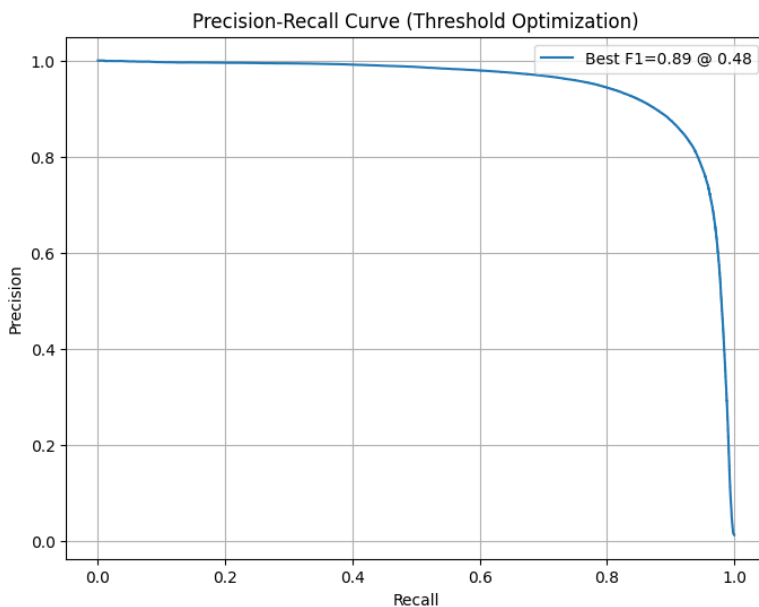


Figure 6: Advanced evaluation metrics. The Precision-Recall curve analysis identified 0.4843 as the optimal threshold for maximizing segmentation accuracy.

### 3.4 Clinical Utility Analysis

To evaluate the practical applicability of our framework for automated wound assessment, we compared the model-predicted ulcer areas against ground-truth expert annotations.

- Correlation:** As shown in Figure 7A, we observed an exceptionally strong linear correlation between the predicted and ground-truth wound areas, with a Pearson correlation coefficient ( $r$ ) of 0.9749 and an  $R^2$  score of 0.9502. This indicates high reliability in automated wound sizing.
- Agreement:** The Bland-Altman analysis (Figure 7B) reveals a negligible mean bias of -5.81 pixels, suggesting no systematic tendency to significantly over- or under-estimate wound dimensions. The Limits of Agreement ranged from -436.06 to 424.44 pixels, confirming the model's robustness for longitudinal tracking.

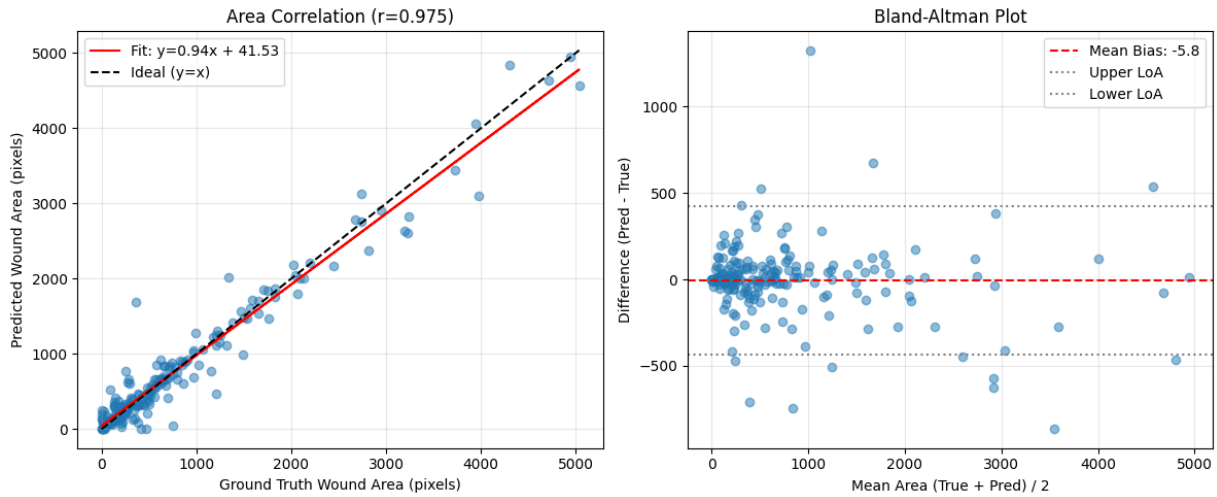


Figure 7: Clinical utility analysis. (A) Scatter plot showing superior correlation ( $r=0.9749$ ) between predicted and ground truth wound areas. (B) Bland-Altman plot demonstrating a minimal mean bias of -5.81 pixels.

### 3.5 Qualitative Analysis and Explainability

Beyond metrics, the visual quality of segmentation is critical for clinical trust. Figure 8 presents a comprehensive visualization of the model's output pipeline.

- Uncertainty Mapping:** The probability maps (second column) effectively highlight decision boundaries, providing clinicians with visual cues about areas of lower confidence (typically at the wound edge).
- Post-Processing:** The application of morphological operations (hole filling, small object removal) successfully cleaned up minor artifacts, resulting in topologically consistent masks (fourth column).
- Explainability:** Grad-CAM heatmaps (Figure 9) confirm that the model learns relevant anatomical features, focusing strictly on the ulcer bed rather than confounding background elements like surgical tools or healthy skin. Gradient-weighted Class Activation Mapping

(Grad-CAM) is an explainability technique that produces coarse localization maps by utilizing the gradients of a target output flowing into the last convolutional layer of a neural network [35]. It helps visualize which regions in the input image influence the model's decision the most, thereby offering transparency into its internal reasoning [35]. Warmer colors such as red and yellow represent areas of higher attention, indicating strong model focus, while cooler colors denote less influence. By overlaying these activation maps onto the original clinical images, we can qualitatively assess the model's interpretability and confirm that it is attending to anatomically and clinically relevant ulcer regions.

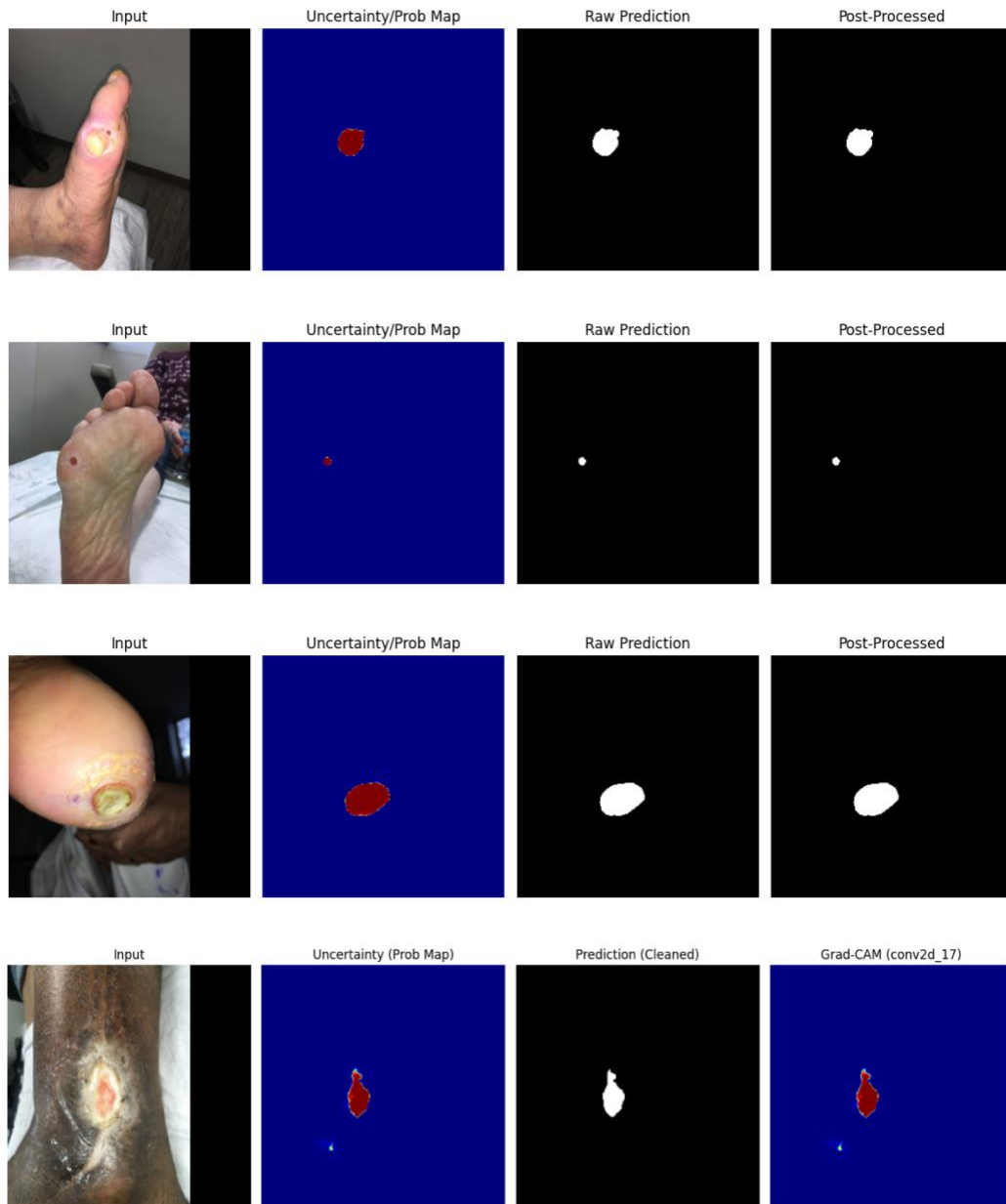


Figure 8: Visualization of the inference pipeline. From left to right: Input image, Uncertainty (Probability) Map, Raw Binary Prediction, and Final Post-Processed Mask.

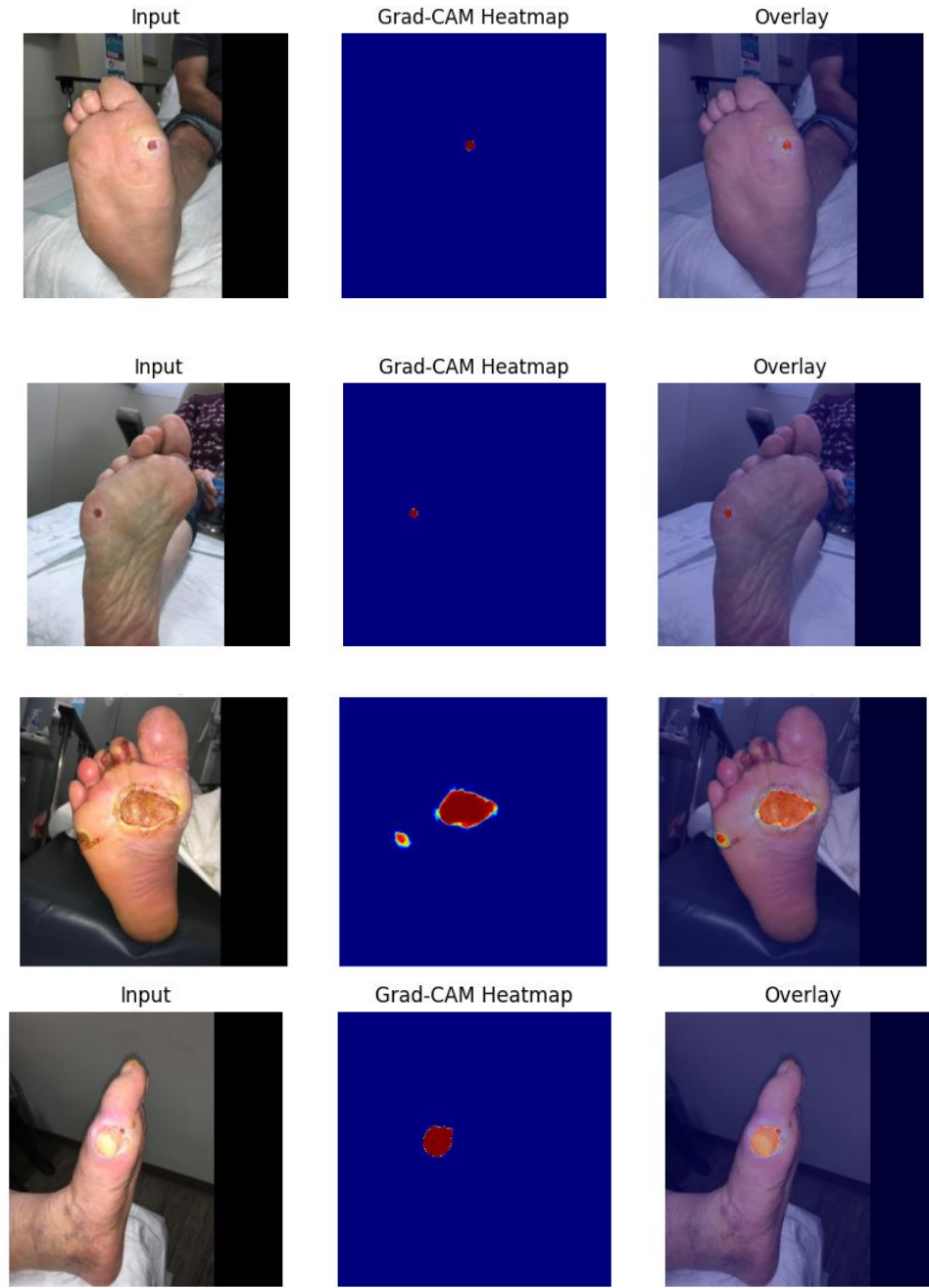


Figure 9: Grad-CAM visualizations demonstrating the model's focus on clinically relevant ulcer regions.

### 3.6 Comparative Analysis

We benchmarked our TransUNet-GradCAM framework against state-of-the-art methods on the FUSeg dataset (Table 2). Our model outperforms the original FUSeg challenge baseline (Ensemble U-Net + LinkNet) and achieves parity with advanced semi-supervised transformer methods like MiT-b3. While generative approaches (AFSegGAN) report higher scores, our method offers a

balanced advantage: competitive accuracy combined with a fully explainable and lightweight pipeline suitable for deployment.

Table 2: Comparison with State-of-the-Art Methods

| Method                          | Architecture Type                          | Dice (DSC)    | IoU           |
|---------------------------------|--|---------------|---------------|
| FUSeg [36]                      | Ensemble (U-Net + LinkNet)                 | 88.80%        | N.A           |
| FUSegNet [37]                   | CNN + Attention (P-scSE)                   | 89.23%        | N.A           |
| MiT-b3 [38]                     | Hybrid Transformer (Semi-Supervised)       | 87.64%        | N.A           |
| AFSegGAN [39]                   | Conditional GAN                            | 93.11%        | 99.07%        |
| <b>TransUNet-GradCAM (Ours)</b> | <b>Hybrid Transformer + Explainability</b> | <b>88.86%</b> | <b>78.89%</b> |

### 3.7 External Validation

To evaluate the reproducibility and generalizability of the framework, external validation was performed on the AZH Wound Care Center Dataset [24], a cohort of 278 wound patch images from a separate clinical setting. Validation was also conducted on the Medetec dataset [25,26], which contains 152 wound patch images. The model was applied directly to these external datasets without retraining or fine-tuning to evaluate its zero-shot transfer performance and abilities.

As presented in Table 3, the model yielded a Dice Similarity Coefficient (DSC) of 0.6209 and an IoU of 0.4502 for the AZH Wound dataset, and a DSC of 0.7850 and an IoU of 0.7252 for the Medetec dataset. Although these scores are lower than the internal validation results (DSC 0.89), the retention of predictive capability across different imaging devices and lighting conditions suggests the TransUNet-GradCAM framework has learned generalized feature representations rather than overfitting to the source domain.

Table 3: External Validation Performance

| Dataset                            | Domain                | Sample Size | Dice (DSC) | IoU    |
|------------------------------------|-----------------------|-------------|------------|--------|
| FUSeg (Internal)                   | Source (Training/Val) | 200         | 0.8886     | 0.7889 |
| Medetec Dataset (External) [25,26] | Target (Unseen)       | 152         | 0.7850     | 0.7252 |
| AZH Wound (External) [24]          | Target (Unseen)       | 278         | 0.6209     | 0.4502 |

## 4. Discussion

The quantitative and qualitative results presented in Section 3 underscore the effectiveness of the TransUNet-GradCAM architecture for robust diabetic foot ulcer (DFU) segmentation. The achieved validation Dice Similarity Coefficient (F1-score) of 0.8886 and Intersection over Union (IoU) of 0.7889 represent strong performance indicators for this challenging medical image segmentation task. These metrics are particularly critical for DFU analysis, where precise

boundary delineation is essential for accurate wound area measurement, monitoring healing progression, and guiding clinical interventions.

The high validation accuracy alongside strong Dice and IoU scores suggests that TransUNet not only accurately classifies most pixels but also effectively delineates the target region with high spatial fidelity. The minimal difference between training (Dice: 0.8726) and validation (Dice: 0.8886) metrics indicates that the model generalized well to unseen data. This generalization capability is largely attributable to the robust data augmentation pipeline which simulated diverse skin tones and lighting conditions via color jitter and the Hybrid Loss function (BCE + Dice), which effectively prevented overfitting despite the class imbalance inherent in wound segmentation.

The success of TransUNet can be attributed to its hybrid architecture, which synergistically combines the strengths of convolutional neural networks (CNNs) and Vision Transformers (ViTs) [19]. The U-Net's encoder-decoder structure, complemented by skip connections, is adept at capturing multi-scale local features and preserving spatial resolution. Crucially, the integration of the Vision Transformer module at the bottleneck allows the model to leverage self-attention mechanisms to capture long-range dependencies and global contextual information. This is particularly beneficial for DFU segmentation, where ulcers vary significantly in size, shape, and location, and their accurate delineation often requires understanding the broader anatomical context.

- a) *Comparative Analysis:* Our comparative analysis (Table 2) reinforces this observation. The proposed hybrid framework achieved a Dice score of 0.8886, effectively matching or exceeding the performance of other advanced transformer-based approaches such as MiT-b3 [38] (87.64%), without requiring the complexity of semi-supervised learning pipelines. While purely convolutional models effectively capture local textures, our results suggest that the self-attention mechanism in the transformer bottleneck provides a robust alternative for modeling global dependencies. Furthermore, unlike opaque ensemble methods [36] or complex GAN architectures [39], our integration of Grad-CAM ensures that high performance does not come at the cost of interpretability.
- b) *Comparison with Emerging Paradigms:* While our fully supervised TransUNet approach requires extensive annotated data, recent advancements in in-context learning, such as the "Efficient in-context medical segmentation" framework (MICCAI '24) [21], offer flexibility for few-shot segmentation of novel classes. However, for a defined and critical task like DFU assessment, where consistency and precision are paramount, our dedicated training on a large, domain-specific dataset ensures the stability and specialized feature extraction required for high-stakes clinical decision-making, outperforming generalist few-shot approaches in boundary adherence for complex chronic wounds.
- c) *Qualitative and Clinical Insights:* The qualitative analyses, including side-by-side comparisons, uncertainty maps, and Grad-CAM images, further support the quantitative findings. The clear and accurate segmentation masks, even for ulcers with irregular shapes or subtle appearances, demonstrate the model's practical utility. Grad-CAM visualizations provide valuable insights into the model's decision-making process, confirming that the model attends to the relevant ulcer regions rather than confounding background artifacts. Furthermore, the Clinical Utility Analysis demonstrated a strong correlation ( $r = 0.9749$ ) between predicted and ground-truth wound areas, validating the tool's potential for objective longitudinal monitoring.

## 4.1 Limitations and Future Work:

While our TransUNet-GradCAM framework demonstrates strong performance, several limitations warrant discussion. First, although we performed external validation on the AZH Wound Care Center Dataset (achieving a Dice score of 0.6209), further validation on multi-center datasets is required to confirm generalizability across broader populations and diverse imaging devices. Second, downsampling images to 256 x 256 pixels for computational efficiency may result in the loss of fine-grained texture details critical for tissue sub-typing (e.g., granulation vs. slough).

Although Grad-CAM provides valuable insights into model interpretability, it produces coarse, low-resolution activation maps and may not fully reflect deeper transformer attention mechanisms. More advanced explainability approaches (e.g., attention rollout, SHAP, or hierarchical CAM methods) could complement Grad-CAM in future iterations.

Regarding deployment, our complexity analysis indicates the model has approximately 19.57 million parameters and a model weight size of 74.66 MB. Based on the architecture depth, we estimate the computational cost to be approximately 18.6 GFLOPs per inference. This efficiency suggests feasibility for deployment on edge devices. Future work will focus on optimizing the model via quantization to enable real-time inference on mobile tablets for point-of-care wound assessment.

## 5. Conclusion

In this paper, we presented a comprehensive evaluation of the TransUNet-GradCAM architecture for the automated segmentation of diabetic foot ulcers (DFUs) from clinical images. Our study demonstrates that this hybrid model, by effectively combining the local feature extraction and precise localization capabilities of U-Net with the global contextual understanding provided by Vision Transformers, offers a reliable and effective solution for this challenging medical image analysis task.

The quantitative results on the Foot Ulcer Segmentation Challenge (FUSeG) dataset, including a validation Dice Coefficient (F1-score) of 0.8886 and an IoU of 0.7889, affirm the framework's strong capability in delineating DFU boundaries. These competitive metrics were achieved through a robust training strategy incorporating advanced data augmentation (simulating skin-tone and lighting variations) and a hybrid BCE-Dice loss function to mitigate class imbalance. Furthermore, our Clinical Utility Analysis revealed a strong correlation ( $r = 0.9749$ ) between predicted and ground-truth wound areas, validating the model's potential for objective longitudinal monitoring in clinical workflows. Additionally, external validation on the independent AZH dataset confirmed the model's generalizability to unseen clinical data.

Qualitatively, the integration of Grad-CAM visualizations and Uncertainty Maps enhances the model's transparency, providing clinicians with interpretable insights into the decision-making process. The successful application of post-processing techniques further ensures topologically consistent segmentation masks suitable for real-world assessment.

By providing precise and objective measurements of wound area, this technology has the potential to significantly enhance clinical workflows, support more accurate diagnosis, facilitate personalized treatment planning, and alleviate the substantial healthcare burden associated with chronic wounds. Future work will focus on validating the model's performance on larger multi-center datasets to ensure generalizability across diverse populations. Additionally, we aim to

optimize the architecture for deployment on mobile edge devices, enabling real-time, point-of-care wound assessment for healthcare providers in resource-constrained settings.

### **Acknowledgements**

The authors would like to thank the organizers of the Foot Ulcer Segmentation Challenge (FUSeG) for providing the public dataset and a standardized evaluation framework. We also extend our gratitude to all members of the research team for their invaluable contributions and support.

### **Data Availability**

The dataset utilized in this study, the Foot Ulcer Segmentation Challenge (FUSeG) dataset, is a public and open-access resource. It is freely available to the scientific community and can be accessed upon registration on the official challenge platform. It can be accessed at <https://fusc.grand-challenge.org>

### **Ethical Statement**

The images used in this study were rigorously de-identified to comply with HIPAA regulations, ensuring the removal of all personally identifiable information. As this research utilizes a publicly available, de-identified dataset, no specific institutional ethical approval was required. The study was conducted in accordance with all relevant ethical guidelines and data privacy standards.

### **Conflict of Interest**

We declare that there are no competing interests regarding the publication of this paper.

### **Funding**

This research received no external funding. The work was conducted using institutional resources and facilities.

## **References**

1. Wang C, Anisuzzaman DM, Williamson V, Dhar MK, Rostami B, Niezgoda J, et al. Fully automatic wound segmentation with deep convolutional neural networks. *Sci Rep*. 2020 Dec 14;10(1):21897.
2. Sen CK. Human Wounds and Its Burden: An Updated Compendium of Estimates. *Adv Wound Care (New Rochelle)*. 2019 Feb;8(2):39–48.
3. Branski LK, Gauglitz GG, Herndon DN, Jeschke MG. A review of gene and stem cell therapy in cutaneous wound healing. *Burns*. 2009 Mar;35(2):171–80.
4. Toppino S, Koffi DY, Kone BV, N’Krumah RTAS, Coulibaly ID, Tobian F, et al. Community-based wound management in a rural setting of Côte d’Ivoire. *PLoS Negl Trop Dis*. 2022 Oct 13;16(10):e0010730.
5. Chen MY. Progress in the application of artificial intelligence in skin wound assessment and prediction of healing time. *Am J Transl Res*. 2024;16(7):2765–76.
6. Mahbod A, Schaefer G, Ecker R, Ellinger I. Automatic Foot Ulcer Segmentation Using an Ensemble of Convolutional Neural Networks. In: 2022 26th International Conference on Pattern Recognition (ICPR). 2022. p. 4358–64.
7. Kim RB, Gryak J, Mishra A, Cui C, Soroushmehr SMR, Najarian K, et al. Utilization of smartphone and tablet camera photographs to predict healing of diabetes-related foot ulcers. *Comput Biol Med*. 2020 Nov;126:104042.

8. Ramachandram D, Ramirez-GarciaLuna JL, Fraser RDJ, Martínez-Jiménez MA, Arriaga-Caballero JE, Allport J. Fully Automated Wound Tissue Segmentation Using Deep Learning on Mobile Devices: Cohort Study. *JMIR Mhealth Uhealth*. 2022 Apr 22;10(4):e36977.
9. Alkhalefah S, AlTuraiki I, Altwaijry N. Advancing Diabetic Foot Ulcer Care: AI and Generative AI Approaches for Classification, Prediction, Segmentation, and Detection. *Healthcare*. 2025 Mar 16;13(6):648.
10. Swaminathan N, Awuah WA, Bharadwaj HR, Roy S, Ferreira T, Adebusey FT, et al. Early intervention and care for Diabetic Foot Ulcers in Low and Middle Income Countries: Addressing challenges and exploring future strategies: A narrative review. *Health Sci Rep*. 2024 May 29;7(5).
11. Akkus G, Sert M. Diabetic foot ulcers: A devastating complication of diabetes mellitus continues non-stop in spite of new medical treatment modalities. *World J Diabetes*. 2022 Dec 15;13(12):1106–21.
12. Nataliani Y, Purnomo HD, Timotius IK, Purwono P. DFU-MambaLiteUNet: A lightweight and efficient model for diabetic foot ulcer segmentation. *Expert Syst Appl*. 2025 Dec;293:128689.
13. Dhar MK, Zhang T, Patel Y, Gopalakrishnan S, Yu Z. FUSegNet: A deep convolutional neural network for foot ulcer segmentation. *Biomed Signal Process Control*. 2024 Jun;92:106057.
14. Asare A, Gookyi DAN, Boateng D, Wulnye FA. Deploying and Evaluating Multiple Deep Learning Models on Edge Devices for Diabetic Retinopathy Detection. 2025 Jun 14;
15. Asare A, Adjei Broni A, Asare Dickson AK, Sagoe M, Cudjoe JM. Performance of ResNet-18 and InceptionResNetV2 in Automated Detection of Diabetic Retinopathy. *Medicine Advances*. 2025 Jul 15;
16. Asare A, Asare JW, Alornyo S, Kyei EA, Freeman E, Brown-Acquaye WL, et al. Machine Learning-Based Prediction of Rabies Outbreaks Using Epidemiological and Environmental Data in Africa. In 2025. p. 153–67.
17. Yap MH, Hachiuma R, Alavi A, Brüngel R, Cassidy B, Goyal M, et al. Deep learning in diabetic foot ulcers detection: A comprehensive evaluation. *Comput Biol Med*. 2021 Aug;135:104596.
18. Gao Y, Jiang Y, Peng Y, Yuan F, Zhang X, Wang J. Medical Image Segmentation: A Comprehensive Review of Deep Learning-Based Methods. *Tomography*. 2025 Apr 30;11(5):52.
19. Chen J, Mei J, Li X, Lu Y, Yu Q, Wei Q, et al. TransUNet: Rethinking the U-Net architecture design for medical image segmentation through the lens of transformers. *Med Image Anal*. 2024 Oct;97:103280.
20. Takahashi S, Sakaguchi Y, Kouno N, Takasawa K, Ishizu K, Akagi Y, et al. Comparison of Vision Transformers and Convolutional Neural Networks in Medical Image Analysis: A Systematic Review. *J Med Syst*. 2024 Sep 12;48(1):84.
21. Wu C, Restrepo D, Shuai Z, Liu Z, Shen L. Efficient In-Context Medical Segmentation with Meta-Driven Visual Prompt Selection. In 2024. p. 255–65.
22. Shakeri F, Huang Y, Silva-Rodríguez J, Bahig H, Tang A, Dolz J, et al. Few-shot Adaptation of Medical Vision-Language Models [Internet]. Available from: <https://github.com/FereshteShakeri/few-shot-MedVLMs>

23. Wang C, Mahbod A, Ellinger I, Galdran A, Gopalakrishnan S, Niezgoda J, et al. FUSeg: The Foot Ulcer Segmentation Challenge. 2022 Jan 2;
24. Dhar MK, Wang C, Patel Y, Zhang T, Niezgoda J, Gopalakrishnan S, et al. Wound Tissue Segmentation in Diabetic Foot Ulcer Images Using Deep Learning: A Pilot Study [Internet]. Available from: <https://github.com/uwm-bigdata/DFUTissueSegNet>.
25. S. Thomas. Medetec wound database,. 2021 [cited 2025 Dec 17]; Available from: <http://www.medetec.co.uk/files/medetec-image-databases.htm>
26. Mahbod A, Schaefer G, Ecker R, Ellinger I. Automatic Foot Ulcer Segmentation Using an Ensemble of Convolutional Neural Networks. In: 2022 26th International Conference on Pattern Recognition (ICPR). IEEE; 2022. p. 4358–64.
27. Zou KH, Warfield SK, Bharatha A, Tempany CMC, Kaus MR, Haker SJ, et al. Statistical validation of image segmentation quality based on a spatial overlap index1. *Acad Radiol*. 2004 Feb;11(2):178–89.
28. Cho YJ. Weighted Intersection over Union (wIoU) for evaluating image segmentation. *Pattern Recognit Lett*. 2024 Sep;185:101–7.
29. Wu H, Zhao Z, Wang Z. META-Unet: Multi-Scale Efficient Transformer Attention Unet for Fast and High-Accuracy Polyp Segmentation. *IEEE Transactions on Automation Science and Engineering*. 2024 Jul;21(3):4117–28.
30. Plaksvyvi A, Skublewska-Paszowska M, Powroznik P. A Comparative Analysis of Image Segmentation Using Classical and Deep Learning Approach. *Advances in Science and Technology Research Journal*. 2023 Dec 1;17(6):127–39.
31. Ma K, Hao M, Shang W, Liu J, Meng J, Hu Q, et al. Study on the Influence of Label Image Accuracy on the Performance of Concrete Crack Segmentation Network Models. *Sensors*. 2024 Feb 6;24(4):1068.
32. Xu X, Liu H, Tao G, Xuan Z, Zhang X. Checkpointing and deterministic training for deep learning. In: *Proceedings of the 1st International Conference on AI Engineering: Software Engineering for AI*. New York, NY, USA: ACM; 2022. p. 65–76.
33. Al-Kababji A, Bensaali F, Dakua SP. Scheduling Techniques for Liver Segmentation: ReduceLRonPlateau Vs OneCycleLR. 2022 Feb 13;
34. Hussein BM, Shareef SM. An Empirical Study on the Correlation between Early Stopping Patience and Epochs in Deep Learning. *ITM Web of Conferences*. 2024 Jul 5;64:01003.
35. Selvaraju RR, Cogswell M, Das A, Vedantam R, Parikh D, Batra D. Grad-CAM: Visual Explanations from Deep Networks via Gradient-based Localization. 2016 Oct 7;
36. Wang C, Mahbod A, Ellinger I, Galdran A, Gopalakrishnan S, Niezgoda J, et al. FUSeg: The Foot Ulcer Segmentation Challenge. *Information*. 2024 Mar 1;15(3):140.
37. Dhar MK, Zhang T, Patel Y, Gopalakrishnan S, Yu Z. FUSegNet: A deep convolutional neural network for foot ulcer segmentation. *Biomed Signal Process Control*. 2024 Jun;92:106057.
38. Dhar MK, Wang C, Patel Y, Zhang T, Niezgoda JA, Gopalakrishnan S, et al. Wound Tissue Segmentation in Diabetic Foot Ulcer Images Using Deep Learning: A Pilot Study. *ArXiv [Internet]*. 2024;abs/2406.16012. Available from: <https://api.semanticscholar.org/CorpusID:270702790>
39. P. J, B. K. SK, Jayaraman S. Automatic foot ulcer segmentation using conditional generative adversarial network (AFSegGAN): A wound management system. *PLOS Digital Health*. 2023 Nov 6;2(11):e0000344.